Generation of highly symmetric, cylindrically convergent shockwaves in water

S. N. Bland,[1] Ya. E. Krasik,[2] D. Yanuka,[2] R. Gardner,[1] J. MacDonald,[1] A. Virozub,[2] S. Efimov,[2] S. Gleizer,[2] and N. Chaturvedi[1]

[1]*Institute of Shock Physics, Imperial College London, London SW7 2BW, United Kingdom*
[2]*Physics Department, Technion - Israel Institute of Technology, Haifa 32000, Israel*

We report on pulsed power driven, exploding copper wire array experiments conducted to generate cylindrical convergent shockwaves in water employing μs risetime currents >550 kA in amplitude and with stored energies of >15 kJ—a substantial increase over previous results. The experiments were carried out on the recently constructed Mega-Ampere-Compression-and-Hydrodynamics facility at Imperial College London in collaboration with colleagues of Technion, Israel. 10 mm diameter arrays consisting of $60 \times 130 \, \mu$m wires were utilized, and the current and voltage diagnostics of the load region suggested that ~ 8 kJ of energy was deposited in the wires (and the load region close to the wires) during the experiments, resulting in the formation of dense, highly resistive plasmas that rapidly expanded driving the shockwaves in water. Laser-backlit framing images of the shockfront were obtained at radii <0.25 mm for the first time, and there was strong evidence that even at radii <0.1 mm this front remains stable, resulting in a convergence ratio of $>50{:}1$. Framing images and streak photographs showed that the velocity of the shockwave reached ~ 7.5 km s^{-1} at 0.1 mm from the axis. 2D hydrodynamic simulations that match the experimentally obtained implosion trajectory suggest that pressures >1 Mbar are produced within 10 μm of the axis along with water densities of 3 gcm^{-3} and temperatures of many 1000 s of Kelvin. Under these conditions, Quotidian Equation of State suggests that a strongly coupled plasma with an ionization fraction of ~ 0.7 would be formed. The results represent a "stepping stone" in the application of the technique to drive different material samples into high pressure, warm dense matter regimes with compact, university scale generators, and provide support in scaling the technique to multi-mega ampere currents. *Published by AIP Publishing.* [http://dx.doi.org/10.1063/1.4994328]

I. INTRODUCTION

The production of highly symmetric, cylindrically convergent pressure waves is appealing for equation of state (EOS) research as they allow high pressures and densities to be reached in relatively compact systems. Several methods for producing convergent shockwaves have been developed, for instance, a highly explosive "jacket"[1–3] or redirection of the planar compression produced in a gas-gun impact.[4] High current pulsed power has also been used to produce "quasi-isentropic" pressure waves, with the current flowing through the outer layers of a liner and interacting with the induced magnetic field to produce compression of the liner.[5] Recent experiments on the world's largest pulsed power accelerator—the 26 MA Z facility at Sandia National Laboratories—have used a highly shaped current pulse to produce quasi-isentropic compression of a liner with a cryogenic deuterium fill to the Gbar level, which was diagnosed by monochromatic X-ray radiography.[6]

The use of convergent geometries on smaller scale pulsed power generators has, so far, been limited. Despite the potential advantages, issues with diagnostics and diagnostic access have restricted most EOS research to be planar in nature, typically utilizing magnetically driven strip lines to peak pressures of a few 10 s–100 s of kbar.[7–9]

Research at Technion has demonstrated a promising new method of producing convergent shockwaves in water that does not rely on magnetic compression, and instead utilizes the electrically driven explosion of arrays of metallic wires.[10,11] The shockwaves produced can be diagnosed optically over a majority of the radius of convergence (typically 5–10 mm) and over durations of 100 s of nanoseconds. Furthermore, the technique places far less stress on the pulsed power generator than magnetic techniques as the load is critically damped i.e. a large fraction of energy stored in the generator is used to explode the wires and produce the shockwaves, so there is no "ringing"/large scale reversal of the current as often observed with inductive loads.

To produce the shockwaves, symmetric arrays of $\sim 100 \, \mu$m metallic wires are placed under water and a sub-μs risetime, several 100 kA current is applied to the wires. The water acts to prevent the breakdown of the wire material along its surface[12,13] (as found in typical wire array z-pinch experiments in a vacuum) and tampers the wire expansion, resulting in very large energies being deposited in the wire material through Ohmic heating—so far energies up to 200 eV per atom have been measured with copper wires.[10] The entire volume of the wire undergoes phase changes, entering a dense, highly resistive gas–plasma mix.[14] The large energies deposited in the wire and its associated change in phase cause it to rapidly expand, launching a uniform, radially expanding shockwave into the surrounding water. With the wires arranged into a cylindrical array, shockwaves from adjacent wires rapidly merge together, forming a highly

symmetric, many kms^{-1} implosion that converges onto the axis of the experiment.

Experiments at Technion have primarily explored cylindrical arrays driven by ∼μs risetime currents with peaks up to 300 kA, which resulted in energies up to 4.5 kJ being deposited in the exploding wires; whilst in some experiments with much faster risetimes of 350 ns and currents of ∼500 kA, ∼6 kJ was deposited in the wires.[10,11] However, there has been little imaging of the shockwaves produced close to the axis of the array, with framing images at ∼0.2–0.3 mm radius only in the lower current experiments. Trajectories of the imploding shockwaves were measured from the framing data at high radii and then inferred from a "time of flight measurement" with the arrival of the shockwave at the axis set to correspond to the onset of increased optical emission seen on photodiodes. These trajectories were compared with hydrodynamic simulations incorporating a high pressure EOS for water and copper which indicated that at implosion of such a shockwave, ∼Mbar pressures would be produced at ∼5 μm radii from the axis, and that the temperature of the water would reach many 1000 s of Kelvin—consistent with the optical emission seen to originate from the axis. The technique has now been extended to produce spherically symmetric implosions[11] where there is good evidence that pressures >10Mbar are produced close to the centre of the implosion. However, key questions related to the stability, symmetry and trajectory of the converging shockwaves at radii smaller than ∼0.2 mm, and the possibility of operating such wire arrays with significantly larger deposited energies remain unanswered. Thus, there is great interest in scaling experiments to larger currents/large driver energies, with better diagnostic techniques that can image the shockwaves closer to the axis.

This paper details the first underwater wire array research with ∼μs risetime currents of amplitude >500 kA. The experiments were carried out on the Mega-Ampere-Compression-and-Hydrodynamics (MACH) generator at Imperial College London[15,16] in collaboration with colleagues of Technion. In Sec. II of this paper, the experimental setup and diagnostics used to measure the shockwaves are described. Section III includes the results and discussion of the experiments. In the first part of Sec. III A, experiments with thick solid copper liners are detailed, which were primarily used to calibrate current and voltage diagnostics positioned relatively close to the load. Despite the lack of a large scale movement of the liner, a shockwave was observed to launch from its inner surface and converge on the axis—the mechanism by which this shockwave formed is still under study. In the second part of Sec. III B, experiments with cylindrical arrays of wires are described. Measurements of the energy resistively deposited in the wires are presented and used to provide evidence of the state of the wire material as the wires explode into dense, resistive, strongly coupled plasmas. Framing images show that the imploding shock-front driven by the wire expansion is highly uniform, and there is strong evidence that convergence ratios >50:1 are obtained. Simple calculations of the pressures at different radii are performed. In Sec. IV, the results of hydrodynamic calculations of the pressure, density and temperature that the

water attains in the final stages of the implosion are presented, based on the implosion trajectories measured in Sec. III B. Comparing these parameters with Quotidian Equation of State (QEOS) models suggests the formation of a high pressure, strongly coupled plasma on the axis. Finally, Sec. V provides a summary, places the work in context with previous results, and briefly discusses future research areas.

II. EXPERIMENTAL SETUP AND DIAGNOSTICS

Experiments were performed on the Mega-Ampere-Compression-and-Hydrodynamics (MACH) pulsed power facility at Imperial College London. MACH is a 100 kV cavity that was designed to produce 2 MA currents with ∼450 ns risetimes when connected to a low inductance (<5 nH) transmission line and load. The cavity was the basis for a much larger Linear Transformer Driver accelerator; however, as no other cavities were made, MACH has been configured as a set of 40 parallel capacitors in series with 20 low inductance switches that connect via a radial feed. In its simplest form, this can be represented as a "lumped" 6 μF capacitance in series with an inductance of ∼20 nH and a resistance of 15 mΩ.

For the experiments described in this paper, the capacitors were charged between 60 and 70 kV—with a stored energy of 10.8–14.7 kJ (the latter being almost twice the stored energy ever used in experiments at Technion). The inductance of the load and the transmission line connected to the cavity were comparatively high (∼25 nH), which strongly affected the overall performance of the system—for instance, in experiments with solid metal liners described in Sec. III A, peak currents were reduced to 5–600 kA and risetimes increased to ∼1000 ns.

The load configuration used for the water shock experiments is shown in Fig. 1. The anode and cathode plates were separated by ∼8 mm during the experiments, and the entire region of the upper surface of the cathode plate to the top of the current return cylinder was flooded with de-ionized water—immersing the wire array. Shock absorbing materials and spring loaded bolts were used throughout the load region, as the shockwaves transmitted through the water were highly damaging—regularly shearing the fixings and bending 10 mm thick stainless steel components, such as the return current can.

The wire arrays used typically consisted of $60 \times 130 \, \mu m$ copper wires, with a diameter of 10 mm and a length of 40 mm. These parameters were chosen based on a combination of previous experiments and hydrodynamic simulations performed at Technion and preliminary experiments at Imperial College. The number of wires was chosen such that to provide good azimuthal symmetry—too few wires and the shockwaves from adjacent wires would not merge into the desired cylindrically symmetric, convergent shockwave travelling towards the axis. The diameter of individual wires was selected to optimize the transfer of the energy supplied by MACH to heating of the wires and driving their subsequent explosion into a highly resistive gas–dense plasma mix. In practice, this was achieved by altering the wire diameter so that the rapid increase in resistance associated with the explosion occurred at 70%–80% of the time of peak current
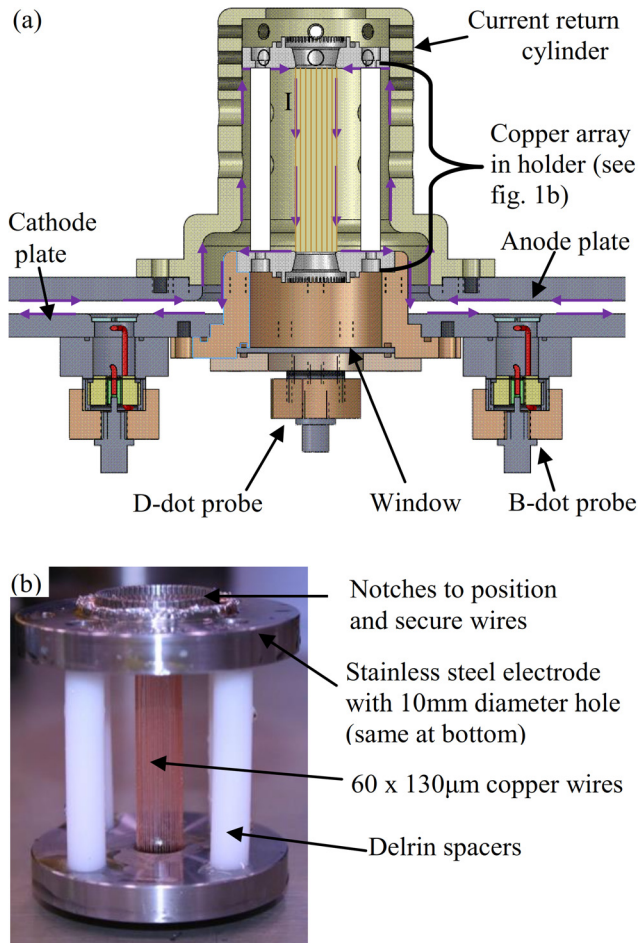
(a)

(b)

FIG. 1. (a) Diagram of the load region on MACH showing connections to the wire array in its holder, together with current (B-dot) and voltage (D-dot) probes. Purple arrows show the direction of conventional current flow—along the anode plate, then the inner surface of the current return cylinder, before travelling through the array holder and array, and heading back along the cathode plate. The anode plate, the return cylinder and the cathode are all made of stainless steel. Note that the D-dot probe is attached to the cathode plate in the same manner as the B-dot probes and at the same distance from the axis, but is "into the page" in the diagram. (b) Picture of a typical wire array in the holder used in the experiments.

in a short circuit experiment. The length of the wires was chosen to ensure that no low resistance plasma channels formed early in the experiment; for example, through electrical breakdown along the surface of the wires, which would limit the heating and explosion of the wires and produce an underdamped oscillation in the current. Finally, the diameter

of the array was set at 10 mm, to ensure that the convergent shockwave was well formed and approaching, but not yet reached, the axis by the time all the possible energy had been transferred to wires.

Current and voltage through the load were measured via two "B-dot" magnetic pick-up coils and one "D-dot" capacitive probe, all placed 15 cm from the axis of the array. Initial experiments utilizing thick, non-imploding copper cylinders (Sec. III A) enabled *in-situ* calibration of these measurements through comparison with a set of "machine diagnostics"— large Rogowski coils placed close to the capacitors.

Dynamics of the shockwaves produced in the experiments were monitored via laser shadowgraphy imaging along the axis of the array, and streak photography across a chord of this (Fig. 2). A 6.5 W 532 nm laser provided backlighting to the shadowgraphy system, and was fiber coupled beneath the load region—preventing any damage to the laser from shockwaves transmitted through MACH. Light from the fiber was collimated into a ~20 mm diameter beam before being fed through the array; thereafter, the array was image relayed to a small optical table. Here, the light was split to an Invisible Vision framing camera with twelve 1024×1024 pixel frames of 5 ns exposure and a Kentech 40 mm optical streak camera backed with a digital single lens reflex camera. Different magnifications, frame timings and streak durations were used in the experiments to highlight both the gross dynamics of the shockwaves and the convergence closer to the axis. Calibration of the exposure times and streak times were performed via a high speed light-emitting diode (LED) pulser; whilst magnifications were calibrated using test objects (e.g., the 1951 USAF resolution slide) placed at the midpoint of the array.

III. RESULTS AND DISCUSSION

A. Calibration experiments with thick copper liners

In order to calibrate the B-dot and D-dot diagnostics close to the load, several experiments were performed using thick copper liners to act as loads of low resistance/constant inductance. Ignoring any capacitive effects in the load region, the current monitored via the B-dots could then be directly compared to measurements by the machine diagnostics. Meanwhile, the voltage across the load measured by the D-dot could be compared with
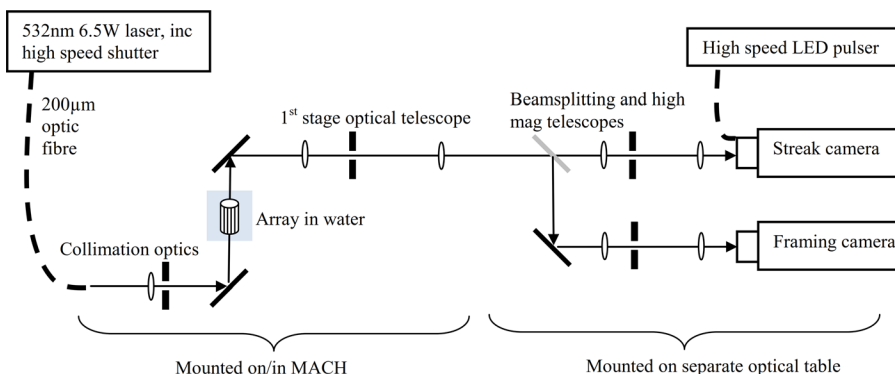

FIG. 2. Schematic of axial diagnostics used in the experiments—CW laser backlit (shadowgraphy) framing images and radial streak photographs.

$$V = IR + L\frac{dI}{dt} + I\frac{dL}{dt}. \qquad (1)$$

The liners used in these experiments had an outer diameter of 9.5 mm and a length of ~50 mm—similar to the diameter and the length of the arrays used in subsequent experiments. The wall thickness of the liner was ~0.9 mm, and after an experiment, there was no obvious change in the outer/inner radii. Neither was there any sign of damage to the inner or outer surfaces, suggesting that any heating of the liner had to be well below its melting point.

A typical current pulse through the liner measured by the machine diagnostics is shown in Fig. 3(a). The pulse has a peak of ~540 kA @1010 ns after the start of the current pulse, and is lightly damped. We can use this to estimate the importance of the terms on the right hand side of Eq. (1). Knowing that the liner does not move, we can assume that the last term tends to zero. Given the liner remains solid, and knowing the frequency of the current pulse (~0.25 MHz), the resistive first term will be much less than the inductive second term throughout the majority of the pulse—except when dI/dt tends to zero at current maxima or minima. Hence, we can use V = L dI/dt during the rising edge of the current pulse to calibrate the voltage measured by the D-dot diagnostic as shown in Fig. 3(b). Here, the inductance was

calculated to be ~27 nH from the geometry of the load region, which compared well with estimates of the inductance made by circuit analysis (25–29 nH) that matched the period of the current waveform in the experiment.

Despite there being no obvious change in the size of the liner after the experiment, laser shadowgraphy images recorded along the axis show that a shockwave still launched from the inside surface of the liner (Fig. 4). The shock is launched at ~460 ns into the current pulse, which then proceeds towards the axis at a constant velocity of ~1.8 km s^{-1}. The shadowgraphy images demonstrate that the shockfront remains symmetric, with the final image at a radius of 0.8 mm, and the implosion continuing beyond this.

The precise mechanism through which the shock is launched from the liner is still being examined. The skin layer in which the current flows ($= \sqrt{2/\sigma\omega\mu}$, where σ is the conductivity, ω the angular frequency and μ the permeability) will be initially ~0.1 mm, much less than the liner thickness of ~0.9 mm. As heating of the liner is limited, this is unlikely to increase significantly on the time scale of the experiment, and current will not reach the inner surface. Similarly, the time taken for conduction to heat the inner surface to >100 °C and cause boiling of the water will also likely be longer than the timescale over which the shockwaves are
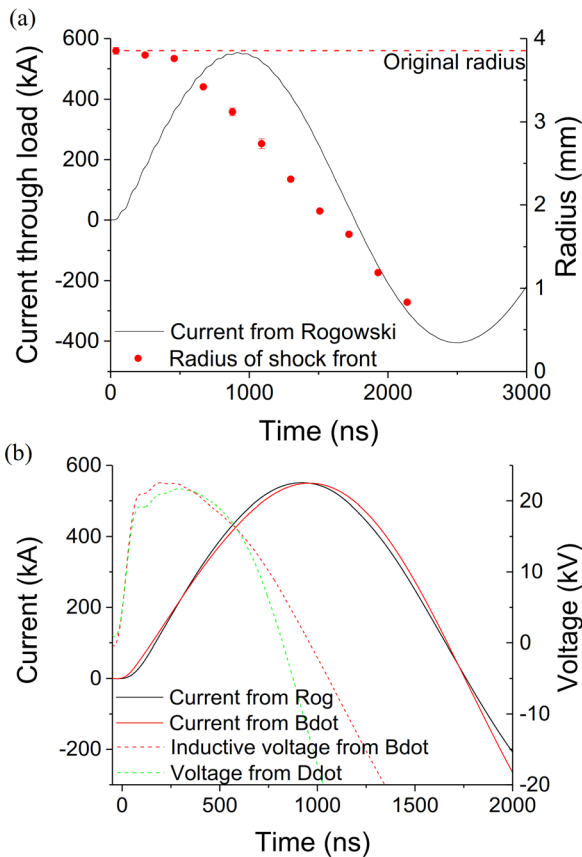

FIG. 3. (a) Current through a solid metal liner used in short circuit tests and trajectory of the shockfront travelling from the inside surface of the liner towards the axis as measured from shadowgraph images. (b) Current measured from Bdot probes near the liner compared with that measured by machine diagnostics (Rog), and voltage measured by the Ddot probe near the liner compared with the 'inductive' voltage calculated from current measurement assuming a constant inductance of 27 nH.
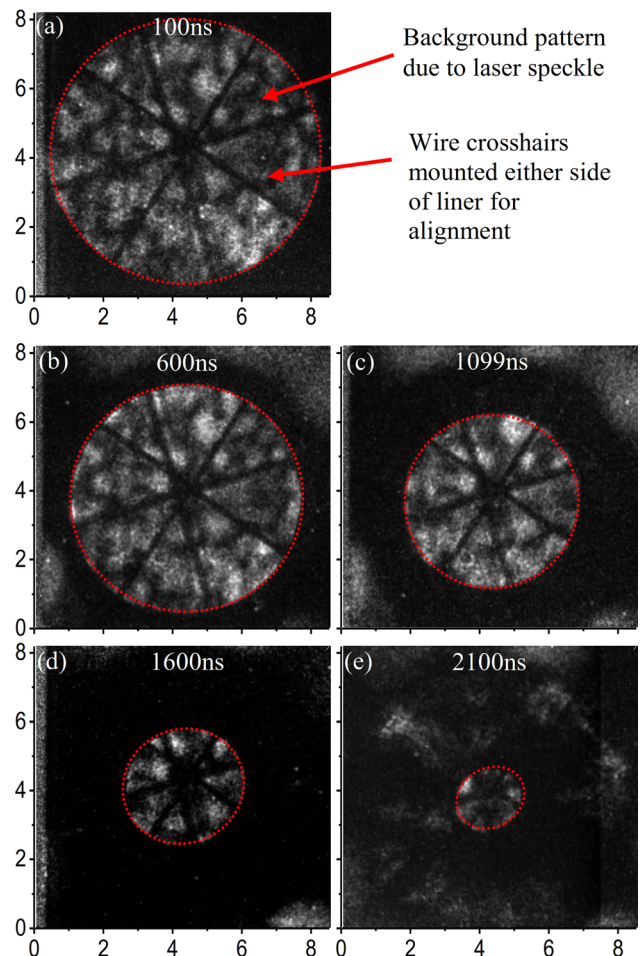

FIG. 4. Shadowgraph images showing the shockwave travelling from the inside surface of the liner towards the axis at (a) 100 ns (b) 600 ns (c) 1099 ns (d) 1600 ns and (e) 2100 ns after the start of current. All axes are in mm. The shockfront is highlighted by the red dotted circle.

observed—besides which boiling is not usually a uniform process, so might not explain the symmetry of the shockfront. A more feasible explanation is the transmission of an increasing pressure wave through the liner into the water. The interaction of the current with its induced magnetic field will result in magnetic pressure, compressing the liner. Given the elastic sound speed in copper is $\sim 4760\,\mathrm{ms^{-1}}$, this pressure wave will take $\sim 190\,\mathrm{ns}$ to transmit through the liner wall; hence, the time at which the shockwave is launched from the inner wall corresponds to the pressure at a time of $460\,\mathrm{ns}$–$190\,\mathrm{ns} = \sim 270\,\mathrm{ns}$ at the outside. At this point, the current is $\sim 190\,\mathrm{kA}$, and so the magnetic pressure ($= B^2/2\mu$) is expected to be $\sim 0.3\,\mathrm{kbar}$. Whilst not high, the impedance mismatch between copper and water could result in a rapid ramp up of the pressure wave into the observed shockwave. We also note that at peak current, the magnetic pressure will be only $\sim 2.6\,\mathrm{kbar}$, which is comparable to the yield strength of copper (typically measured to be ~ 0.7–$3\,\mathrm{kbar}$ depending on how the copper has been formed/alloyed), and so the liner could be behaving elastically, not plastically, resulting in the lack of any measurable change to the liner inner/outer diameter after an experiment.

Whilst not being as fast as the shockwave that reaches the axis when launched from wire arrays (as described in Sec. III B), the phenomena of shockwaves launched from the inner surface of the liner could also have specific uses. For instance, as the liner remains intact during the experiment, the system could be coupled to a repetitive pulsed power generator and used to launch multiple smaller shockwaves through media for material processing or even food preparation.[17]

B. Experiments with wire arrays

The current through and voltage across in a typical experiment utilizing a wire array load is shown in Fig. 5(a). There are immediate differences compared with the liner experiments. In particular, the current shows a peak of $\sim 500\,\mathrm{kA}$ at only $620\,\mathrm{ns}$, and demonstrates little sign of reversal—i.e., the resistance of the wires as they heat up and undergo phase changes has critically damped the current pulse.

Returning to Eq. (1), and assuming that the 3rd term remains zero (i.e., for the duration of the experiment, the current remains concentrated at/close to the original position of the wires), we have $V = IR + L\,dI/dt$. Using the calculated value for the inductance of the array ($\sim 25\,\mathrm{nH}$, similar to that used in the liner experiments), we can use the current measured in the experiment to split the voltage signal into resistive and inductive components, as shown in Fig. 5(b). This demonstrates that the resistive part of the voltage signal spikes to 60–$65\,\mathrm{kV}$ just after peak current i.e., when the inductive component is minimal.

These measurements enable the state of the material from the wires to be determined. Integrating the resistive component with the current through the array, $\int IV_{\mathrm{resistive}}\,dt$ gives the energy dissipated in the array as $8 \pm 0.7\,\mathrm{kJ}$ [Fig. 5(c)], where the error is determined by a combination of noise, uncertainties in the inductance, and hence uncertainties in the calibration of
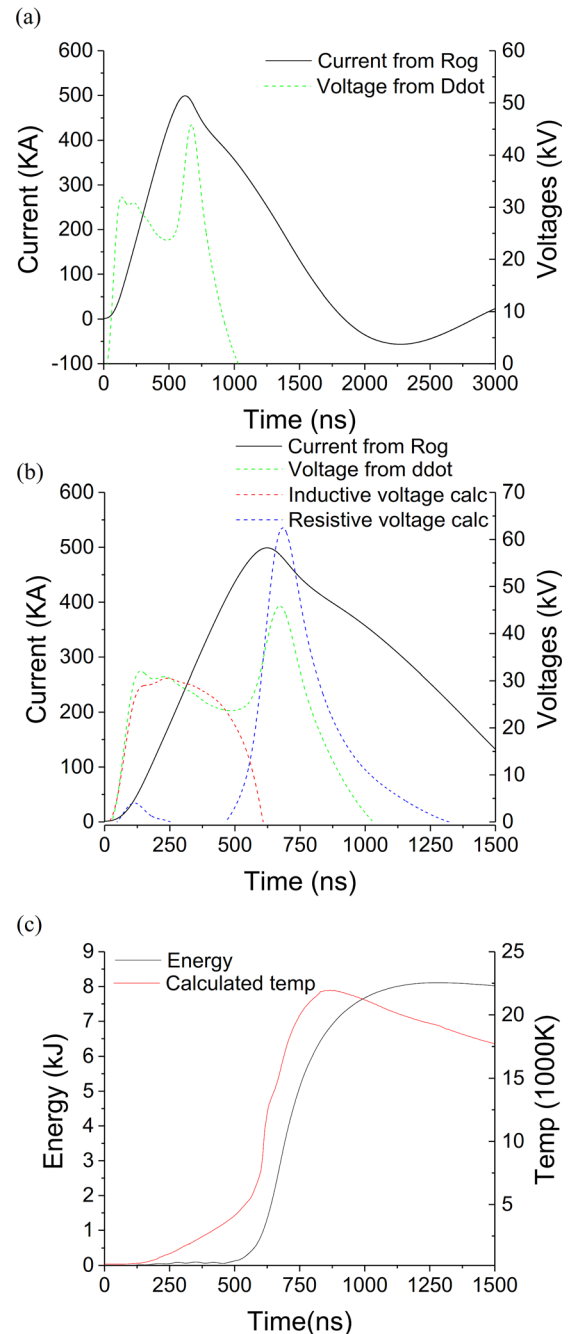

FIG. 5. (a) Current flowing through the array measured by machine diagnostics and voltage across the array measured by the Ddot probe. (b) Close-up of the first peak of current along with voltage measurement from Ddot, the "inductive voltage" calculated from the current signal assuming a constant inductance and the "resistive voltage," the difference between the measured voltage and the inductive voltage calculation. Note that the small rise and fall seen at the resistive voltage around $100\,\mathrm{ns}$ is due to noise in the early time measurements of voltage from the Ddot probe (c) Calculation of energy deposited resistively in the array during experiment ($= \int IV_{\mathrm{resistive}}\,dt$), along with the temperature of the wire material from high resolution simulations using measured current and voltage from the experiment as inputs.

the D-dot probe. At the peak voltage, the resistance of the array is $\sim 0.12\,\Omega$, so the resistance of each wire has reached $\sim 7\,\Omega$. This is significantly more than the initial value of $0.05\,\Omega$ expected at room temperature. The current and resistive voltage were used as inputs to high resolution MHD simulations of a wire/surrounding water to calculate the temperature and

density of the wire material—such simulations have been calibrated against previous single wire data from Technion.[14] The temperature of the wire is shown along with the dissipated energy in Fig. 5(c), and suggests that melting would start at ∼280 ns, and boiling at ∼400 ns. Throughout this time, resistance is increasing, initially in a linear fashion with temperature, whilst the wire is solid, and then exponentially as the wire turns into a liquid. At the peak of energy deposition, calculations suggest that a temperature of 22 000 K/2 eV is reached and the copper will have an ion density of ∼5×10^{20} cm^{-3}. A Quotidian Equation of State (QEOS) model of copper, based on the Franfurt model,[18] suggests that at this point the ionization fraction will be ∼0.5 i.e., a partially ionized, strongly coupled plasma has been formed.

Shadowgraph images along the axis of the array show a highly symmetric, cylindrically converging "shockwave" travelling towards the axis—see Fig. 6. Tracking the position of the shockfront with time demonstrates that this appears to have been launched relatively early in the experiment within ∼50 ns of the start of the current pulse. Until it reaches a radius of 2.5 mm, at a time of 1.7 μs (i.e., long after the peak current), the velocity of the shockfront remains at ∼1.5 km s^{-1}. This corresponds to the speed of sound in water, suggesting that little energy will be required to drive this weak "shockwave" or sonic wave. A similar weak shockwave/sonic wave launched early in time has been obtained in both single wire and wire array studies at Technion.[10] There are several possible explanations to how this wave is formed. It could be due to the still solid copper wires undergoing elastic–plastic transitions driven by magnetic pressure—even at only 50 ns into the current pulse, the field around the wires will already have a magnetic pressure of ∼10 kBar, well above the yield strength of copper. Alternatively, the increased magnetic field around the wires (compared with that around the liners) might result in magnetic diffusion becoming highly non-linear and current melting the surface of the wires earlier than expected. Finally, the surface of any wire will always have some contamination/oxidation, and this could rapidly vaporise.

At ∼1.7 μs, the velocity of the shockfront suddenly increases to ∼3.5 km s^{-1}, and this new velocity remains constant until a radius of ∼0.5 mm. Higher magnification images, such as those shown in Fig. 7, demonstrate that throughout this time the shockfront remains highly uniform and symmetric. Tracking the trajectory of the shockfront back to the radius of the wire array suggests that this higher speed is due to a shockwave that is launched when the wires are expected to boil, ionize and explode, and energy deposition in the array rapidly increases.

As the shockfront gets within ∼0.3 mm of the axis, measurements of symmetry become more challenging as laser speckle—the mottle pattern seen in Figs. 6 and 7—becomes difficult to account for, and any small deviations in the light from the probing laser could easily result in images being clipped. Nevertheless, images [Fig. 7(d/e)] show a near circular pattern of light being transmitted along the axis of the array down to a radius of 0.1 mm—a 50:1 radial convergence.
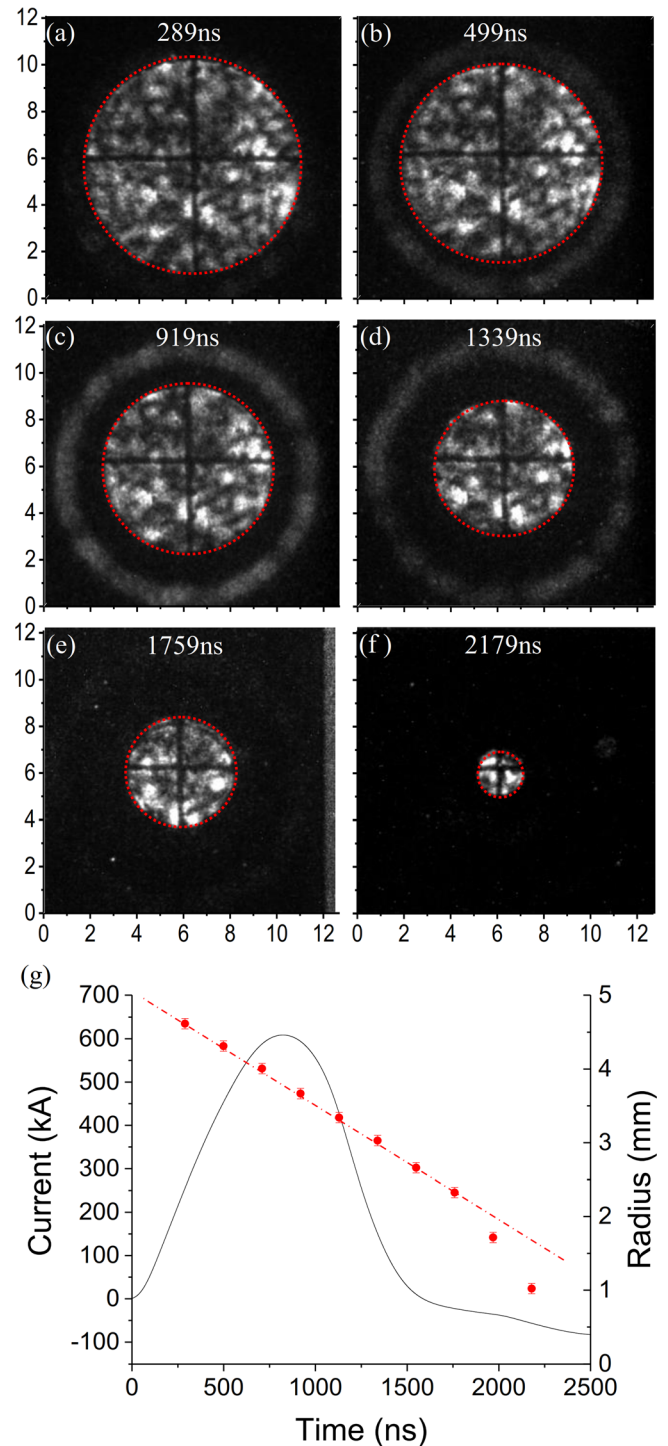

FIG. 6. (a)–(f) Shadowgraph images of the shockwave imploding towards the axis of the array @289 ns, 499 ns, 919 ns, 1339 ns, 1759 ns and 2179 ns after the start of current respectively. The shockfront is highlighted by the red dotted circle, and the axes are all in mm. (g) Current through the array and the trajectory of shockfront travelling towards the axis, as measured from the images.

In several experiments, laser-backlit optical streak photography across a chord of the array was used to supplement the shadowgraph imaging over the last ∼2 mm radius of the array. The position of the shockfront recorded in the streaks—e.g., Fig. 8(a)—overlaid measurements made via the shadowgraph images. Within a radius of 0.5 mm, both streak photography and shadowgraphy show
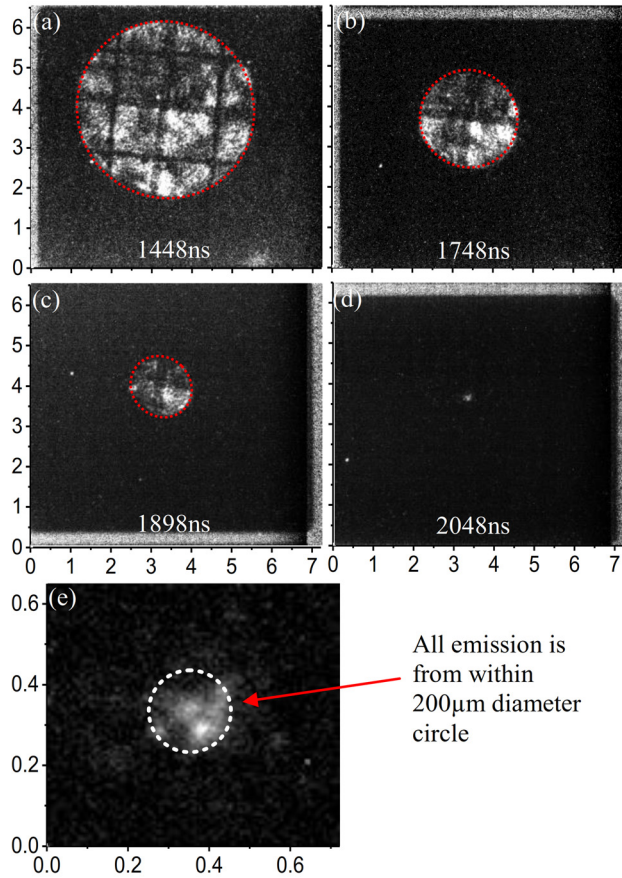
FIG. 7. Higher magnification shadowgraph images of the shockwave at the centre of the array at (a) 1448 ns (b) 1748 ns (c) 1898 ns and (d) 2048 ns after the start of the current pulse. The shockfront is highlighted by the red dotted circle, and the axes are all in mm. (e) Shows a zoomed in view of (d), with a 200 μm diameter circle overlaid.

that the shockfront continually accelerates, reaching a velocity of $\sim$7.5 kms^{-1} at 0.1 mm radius. This acceleration is due to the increase of the pressure behind the shockfront with the decrease in the cross-sectional area of the shock.[19,20]

When/shortly after the shock reaches the axis, there is a small increase in the intensity recorded across the entire radius of the streak image. This most likely corresponds to the rapid heating and ionization of materials on the axis, which will emit into 4π along the length of the array (so is not localized on the streak image). Such an increase in emission has been seen in photodiodes collimated to view the axis of the array in experiments at Technion,[10] where the increase in emission is used to determine the time of flight of the shockwave.

We can use observations of the implosion trajectory to estimate the pressure behind the shockwave. As discussed in Refs. 19 and 21, a self-similar solution to the implosion of a shockwave can be found by relating the radius of shockfront to the time using $R(t_{imp} - t) = A(t_{imp} - t)^{\alpha}$, where t_{imp} is the time of implosion, A is a constant determined by initial conditions and the method of shockwave generation, and α is a factor that depends on geometry which equals 0.75 for cylindrical systems. Using the conservation laws of momentum and energy, and assuming that the shockwave is strong,
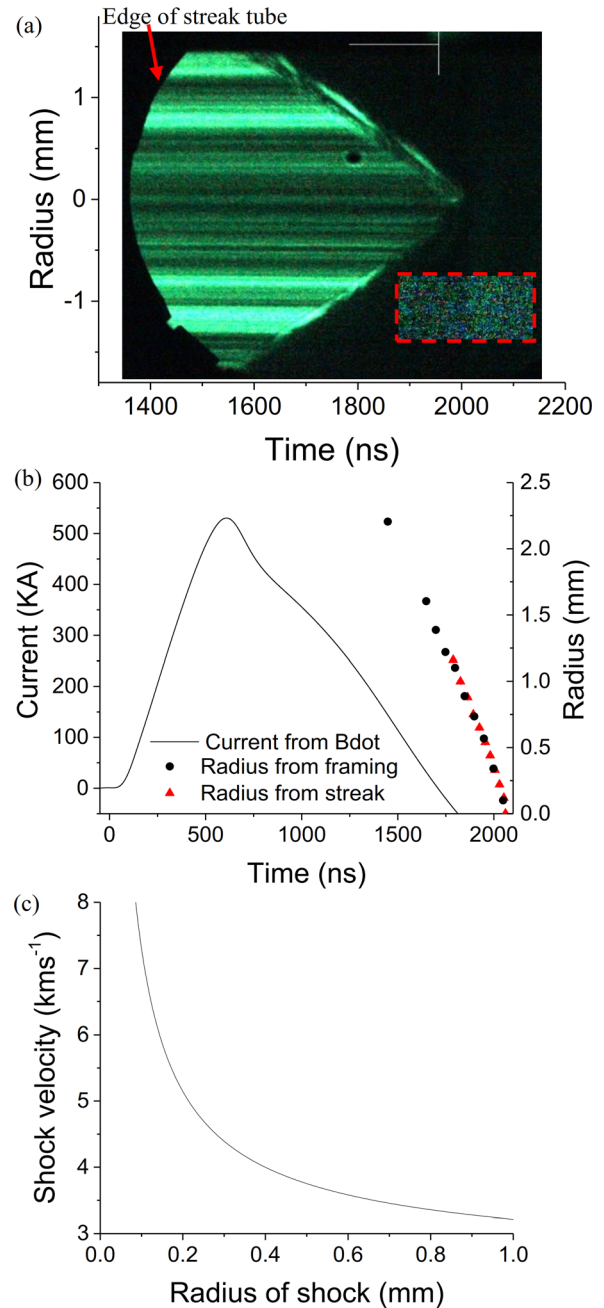

FIG. 8. (a) Laser-backlit streak photograph of the central part of an array showing the shockwave arriving on the axis. The red dashed box shows an area of the image with enhanced brightness and contrast demonstrating that an increase in intensity is observed at/just after arrival of the shock. (b) Trajectory of shockfront as measured from shadowgraph images and streak photographs. (c) Velocity of the shockfront vs. radial position derived by fitting a trajectory to the images and streak data.

enables the pressure immediately behind the shockfront to be estimated as[19,21]

$$P = 2\frac{\rho_o U_s^2}{(\gamma + 1)}, \qquad (2)$$

where U_s is the shock velocity, ρ_0 is the initial water density and γ is the adiabatic index. At 0.1 mm radius, using $U_s = 7.5$ km s^{-1} and $\gamma = 7.15$, the pressure is calculated to be $\sim$140 kbar. The similarity approach then estimates the pressure behind the shockfront at a radius of 10 μm as

$$P_{10\,\mu m} = P_{100\,\mu m} \left(\frac{10 \times 10^{-6}}{100 \times 10^{-6}} \right)^{2-\frac{2}{\alpha}}. \qquad (3)$$

Hence, at $10\,\mu m$, provided that the shock remains stable and uniform, we would expect a pressure of ~ 650 kbar behind the shock. Below a radius of $\sim 10\,\mu m$, simulations suggest that radiation from the heated material behind the shockfront becomes important, and it is difficult to continue using the same self-similar approach.

IV. SIMULATIONS OF THE SHOCKWAVE IMPLOSIONS

2D r-θ Lagrangian hydrodynamic simulations were compared with the trajectory of the shockwave to estimate the parameters including the pressure, density, temperature and energy density in water behind the shock.[22,23] The simulations were based on the finite volume method and included the conservation of mass, momentum and energy coupled with high pressure equations of state for copper and water.

The array parameters ($60 \times 130\,\mu m$ copper wires of diameter 10 mm and length 40 mm) were used as input to the calculations, along with the measured power dissipated in the array found from $IV_{resistive}$. For efficiency, only $1/4$ of the array was simulated with periodic boundary conditions. A Delaunay triangulation method was used, with an initial mesh that varied from a characteristic scale of $\sim 60\,\mu m$ in the vicinity of the wires down to $\sim 5\,\mu m$ close to the axis. Each triangle in the mesh contained information on the pressure, temperature, density and specific energy, and the nodes contained information on the position, velocity and acceleration. Numerical convergence tests were performed to ensure that the simulated values were stable.

In order to match the implosion trajectory of the shockwave within the last ~ 2 mm of the radius, only $\sim 75\%$ of the input power calculated from $IV_{resistive}$ was used in the

simulations. A higher value and the implosion time would be significantly faster and vice-versa. This is consistent with previous results from Technion, and the 25% difference represents several factors: $\sim 5\%$–10% may be accounted for by resistive losses in the connections of the electrodes (which are also measured by the current and voltage probes); there are small systematic errors in the fit to the $IV_{resistive}$ data in the simulations, again at the 5%–10% level; and the remainder of the difference is due to small uncertainties in the implosion trajectory and losses through lower resistivity plasma at the interface of exploding wires and water.

The results of simulations are shown in Fig. 9. The simulations suggest that at the time the shockwave reaches the axis, the water behind the shockwave will attain a pressure >1 Mbar/100 GPa, and this will continue to rise closer to the axis. The density of water will reach nearly $3\,\mathrm{gcm^{-3}}$, $3\times$ its standard value; whilst the temperature will reach many 1000 s of Kelvin, with $>10\,000$ K on the axis—these conditions are consistent with the sudden burst of optical emission observed by the streak camera, shortly after the implosion occurs. The energy density, in the water, meanwhile, becomes 30–40 MJ/kg. Given the high pressures produced, a QEOS model was again used to calculate the ionization states from the conditions predicted in the simulations. This suggested that at the time of implosion, hydrogen in water would attain an ionization fraction of 0.7 within a radius of $10\,\mu m$, and later in time, as the stagnated material releases the ionization fraction at $50\,\mu m$ radius one would reach similar values.

V. SUMMARY, COMPARISONS TO PREVIOUS DATA AND FUTURE RESEARCH AREAS

We have successfully performed the first pulsed power driven, exploding underwater wire array experiments utilizing
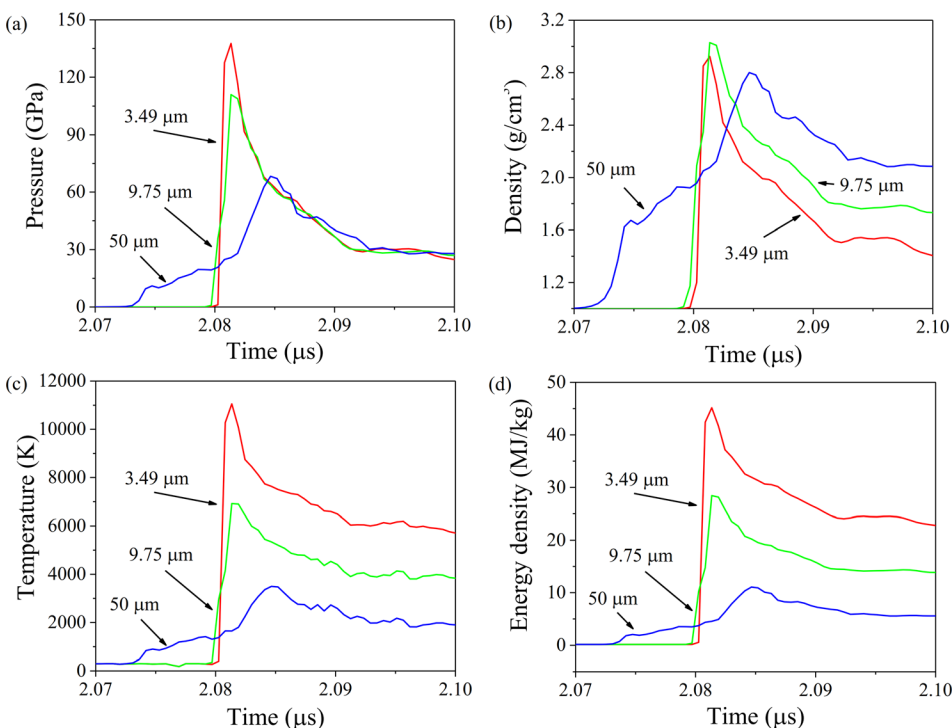
FIG. 9. Simulations of the experimental conditions made with a 2D Lagrangian hydrodynamics code (a) is the pressure in the water (b) is the density of the water (c) is its temperature and (d) is the energy density in the water, all vs. time at different distances from the axis.

$\sim \mu$s currents >500 kA and driving energies >15 kJ. The energy deposited in the wires during these experiments was determined to be ~ 8 kJ.

Shadowgraph images of the implosion demonstrate that it remains stable and uniform until at least 0.35 mm radius, and we have obtained the first images of the implosion below 0.2 mm, providing strong evidence that the implosion remains stable until <0.1 mm from the axis, with a compression ratio of at least 50:1.

The implosion trajectory of the shockfront shows 2 distinct parts. For the majority of the experiment, until it reaches a radius of ~ 2 mm, the shockfront has a velocity of only 1.5 km s^{-1}. It would appear that this initial weak shockwave/sonic wave is launched close to the start of the experiment. From a radius of ~ 2 mm, the shockfront suddenly increases in velocity to ~ 3.5 km s^{-1}. This is associated with a much stronger shockwave launched from the wires, as they were undergoing very rapid Ohmic heating and converting to an expanding vapor–plasma mix. Within the last 0.5 mm radius, the implosion trajectory is seen to continue to accelerate towards the axis, due to the effects of convergence. Using a combination of shadowgraphy images and streak photographs, velocities of ~ 7.5 km s^{-1} were measured at 0.1 mm from the axis.

2D numerical simulations that match the implosion trajectory suggest that pressures of >1 Mbar are produced within 10 μm of the axis, with water densities of 3 g/cc and temperatures of many 1000 s of Kelvin. Under these conditions, QEOS calculations suggest that the water will become partially ionized, forming a strongly coupled plasma. Plasma under such conditions is often referred to as warm dense matter, and typical experiments to produce and analyse plasmas under these conditions usually take place at large national facilities.

Comparing the results of these experiments to previous work for scaling purposes can prove difficult due to the multiple different pulsed power generators previously utilized and the design of the arrays being varied to couple to these generators—with typically smaller wires being used at lower currents, and smaller diameter arrays at faster current risetimes. However, we can draw some simple conclusions:

(i)   Until these experiments, the greatest deposited energy with arrays driven by similar rise-time currents was 4.5 kJ; and at shorter risetime (350 ns) currents was 6 kJ. Prior to this research, one of the biggest concerns was whether significantly increasing the current/ energy deposited in the wires would adversely affect the properties of the wires as they expanded into dense, highly resistive plasma columns—this was particularly worrying at longer current risetimes as breakdown processes are stochastic. This does not appear to be the case, which bodes well for the use of the technique with larger, higher energy generators at multi-MA currents to produce yet higher peak pressures.

(ii)   Despite the high current and relatively long risetimes, the first images of the imploding shockwave at radii of ~ 0.1 mm (half of that previously achieved) provide strong evidence that the shockfront remains stable. The trajectory of the implosion has also been directly measured at these radii for the first time, showing that the trajectory behaves as expected from simulations, with rapid acceleration in close proximity to the axis.

(iii)   In some of the closest experiments to our conditions[24]—with arrays of 40×100 μm copper wires of diameters of 10 mm and lengths of 40 mm, driven by currents of 250 kA—a combination of experimental measurements at larger radii, time of flight data and simulation suggested that the velocity of the shockwaves was ~ 3.4 km s^{-1} at 300 μm radius and 5.5 km s^{-1} at 50 μm radius. Both are lower than the measured velocity in our experiments, which is ~ 4.4 km s^{-1} at 300 μm radius, and even at 100 μm is ~ 7.5 km s^{-1} and continue to accelerate. As the velocity is significantly higher, we would then expect a higher pressure/density/temperature plasma to be produced on the axis.

(iv)   In the experiments described in (iii) above, only ~ 1 kJ was measured as being deposited in the wires, so with "simple" scaling arguments (a factor of $\times 8$ in deposited energy), one would expect $\sim 3\times$ the shock velocity seen in (iii) to be observed in our experiments. In reality, scaling is far more difficult due to the compressibility of the water as the shockwave travels through it. We note though that by using the same simulations used for experiments at lower currents on Technion, and with the same input parameters as these simulations (a fraction of deposited power), we are able to recreate the implosion trajectory of the shockwave and the time of arrival on the axis. This again provides confidence in using the same simulations to plan for experiments at much higher currents and with different risetimes.

Over the next few years, the research will be extended in several ways. Whilst there is now good evidence to show that the use of underwater wire arrays will scale to higher currents/larger driver energies, it is clear that further data are required under these conditions—in particular, experiments must be performed to optimize array design here. We note here that despite MACH having a stored energy of ~ 15 kJ, only ~ 8 kJ was deposited in the wires. This is less than the best experiments at Technion, in which drivers with a stored energy of 8 kJ deposited 6 kJ in the wires. To explore this, new load designs and transmission line hardware on MACH will significantly reduce its inductance, increasing the current in future experiments to the mega-ampere level, whilst reducing the risetime of the current pulse. Simultaneously, improvements in the diagnostics—both electrical and optical—are being planned to increase the accuracy of current and voltage data and enable the trajectory of the shockwave to be more readily followed to smaller radii. To diagnose the state of the material produced on the axis, meanwhile, a combination of time and space resolved optical spectrometry and high-resolution phase contrast X-ray probing is being arranged, the later either being provided by a separately driven X-pinch[25] and/or through transport of MACH to a synchrotron facility.

In addition to cylindrical experiments in water, we will explore the use of other materials, including plastics and cryogenic gases. Here, the question of whether a highly resistive plasma channel can still be obtained from the wires will be paramount.

Finally, we will study different array geometries. The use of spherical arrays in water has been explored at Technion, resulting in far higher pressures expected on the axis. Already, the possibility of using these spherical implosions in water to drive small bubbles of deuterium/tritium fuel for neutron production has been discussed.[21] Exploring the use of a spherical array directly in a cryogenic deuterium bath could prove to be a less complicated route to neutron production and/or would enable estimation of the fusion cross-section to be made under this high pressure, high density, but low temperature parameter space, where quantum tunneling and coulomb screening effects become increasingly important,[26] and the present estimates of the cross-section vary from $\sim 1 \times 10^{-35}$ to 1×10^{-50} cm^{-2}. Spherical arrays though—even more so than cylindrical systems—limit access for diagnostics. Hence, we will explore new geometries such as hemi-spherically bent wires to enable the shockwaves to be more readily studied and to enable their use in driving separate experiments. Work will also commence on producing quasi-isentropic compressions by launching a succession of shockwaves from differently spaced wires.

ACKNOWLEDGMENTS

[1]V. E. Fortov, R. I. Ilkaev, V. A. Arinin, V. V. Burtzev, V. A. Golubev, I. L. Iosilevskiy, V. V. Khrustalev, A. L. Mikhailov, M. A. Mochalov, V. Y. Ternovoi, and M. V. Zhernokletov, Phys. Rev. Lett. **99**, 185001 (2007).

[2]G. R. Fowles and W. M. Isbell, J. Appl. Phys. **36**, 1377 (1965).

[3]Z. Gu, H. Luo, H. Zhang, S. Zhao, X. Tang, Y. Tong, Z. Song, F. Tan, J. Zhao, and C. Sun, J. Phys.: Conf. Ser. **500**, 142018 (2014).

[4]A modification of the scheme described in D. R. Jones, D. E. Eakins, P. J. Hazell, D. J. Chapman, and G. J. Appleby-Thomas, AIP Conf. Proc. **1426**, 1141–1144 (2012).

[5]Such as those described in M. R. Martin, R. W. Lemke, R. D. McBride, J. P. Davis, D. H. Dolan, M. D. Knudson, K. R. Cochrane, D. B. Sinars, I. C. Smith, M. Savage, W. A. Stygar, K. Killebrew, D. G. Flicker, and M. C. Herrmann, Phys. Plasmas **19**, 056310 (2012).

[6]P. F. Knapp, M. R. Martin, D. H. Dolan, K. Cochrane, D. Dalton, J.-P. Davis, C. A. Jennings, G. P. Loisel, D. H. Romero, I. C. Smith, E. P. Yu, M. R. Weis, T. R. Mattsson, R. D. McBride, K. Peterson, J. Schwarz, and D. B. Sinars, Phys. Plasmas **24**, 042708 (2017).

[7]J. R. Asay, T. Ao, J. P. Davis, C. Hall, T. J. Vogler, and G. T. Gray, J. Appl. Phys. **103**, 083514 (2008).

[8]G. Avrillaud, L. Courtois, J. Guerre, P. L. Hereil, F. Lassalle, F. Bayol, P. L'Eplattenier, B. Kovalchuck, E. Kumpjak, N. Zoi, and A. Kim, Dig. Tech. Pap. - 14th IEEE Int. Pulsed Power Conf. **2**, P913–P916 (2003).

[9]C. Sun, G. Wang, C. Liu, J. Zhao, F. Tan, G. Wang, J. Mo, N. Zhang, J. Jiang, and J. Chen, in Proceedings of the Conference of the American Physical Society Topical Group on Shock Compression of Condensed Matter, AIP 978-0-7354-0469-4/07/1196 (2007).

[10]Y. E. Krasik, A. Grinenko, A. Sayapin, S. Efimov, A. Fedotov, V. T. Gurovich, and V. I. Oreshkin, IEEE Trans. Plasma Sci. **36**, 423 (2008), and references therein.

[11]Y. E. Krasik, S. Efimov, D. Sheftman, A. Fedotov-Gefen, O. Antonov, D. Shafer, D. Yanuka, M. Nitishinskiy, M. Kozlov, L. Gilburd, G. Toker, S. Gleizer, E. Zvulun, V. T. Gurovich, D. Varentsov, and M. Rodionova, IEEE Trans. Plasma Sci. **44**, 412 (2016), and references therein.

[12]A. Grinenko, V. T. Gurovich, and Y. E. Krasik, J. Appl. Phys. **100**, 113309 (2006).

[13]A. Fedotov, D. Sheftman, V. T. Gurovich, S. Efimov, G. Bazilitski, Y. E. Krasik, and V. I. Oreshkin, Phys. Plasmas **15**, 082704 (2008).

[14]D. Sheftman, D. Shafer, S. Efimov, and Y. E. Krasik, Phys. Plasmas **19**, 034501 (2012).

[15]S. N. Bland, K. H. Kwek, K. Omar, S. Stafford, J. Winters, and G. Wang, "Bulletin APS topical conference on the shock compression of matter," Bull. Am. Phys. **60**, 8 (2015).

[16]S. N. Bland, K. H. Kwek, R. Gardner, D. Hinshelwood, G. Burdiak, K. Omar, J. Skidmore, R. B. Spielman, S. Stafford, J. Winters, and G. Wang, "MACH: A 2MA generator for compression experiments," Phys Rev. Accel. Beams (unpublished).

[17]F. Garcia and R. Woodall, U.S. patent 6264543 B1 (3 July 2000).

[18]See http://th.physik.uni-frankfurt.de/~faik/feos.php?lang=eng for As developed by Dr Steven Faik of Frankfurt University, with code details/ download packages (last accessed April 12, 2017).

[19]Y. B. Zeldovich and Y. P. Raizer, *Physics of Shock Waves and High-Temperature Hydrodynamic Phenomena*, 2nd ed. (Academic Press, New York, 1967), Vol. 2.

[20]G. B. Whitham, *Linear and Nonlinear Waves* (John Wiley & Sons, Inc., New York, 1974).

[21]A. Grinenko, V. T. Gurovich, and Y. E. Krasik, Phys. Plasmas **14**, 012701 (2007).

[22]I. V. Oreshkin, R. B. Baksht, A. Y. Labezkii, A. G. Rousskikh, A. V. Shishlov, P. R. Levashov, K. V. Khishchenko, and I. V. Glazyrin, Tech. Phys. **49**, 843 (2004).

[23]A. Grinenko, Y. E. Krasik, S. Efimov, A. Fedotov, V. T. Gurovich, and V. I. Oreshkin, Phys. Plasmas **13**, 042701 (2006).

[24]S. Efimov, A. Fedotov, S. Gleizer, V. T. Gurovich, G. Bazalitski, and Y. E. Krasik, Phys. Plasmas **15**, 112703 (2008).

[25]S. A. Pikuz, D. B. Sinars, T. A. Shelkovenko, K. M. Chandler, D. A. Hammer, G. V. Ivanenkov, W. Stepniewski, and I. Yu. Skobelev, Phys. Rev. Lett. **89**, 035003 (2002).

[26]As discussed in report AD-A 214 010, see C. L. Leakeas, Tunneling Effects on Low Energy Fusion Cross Sections, Astronautics Laboratory, Edwards Air Force Base, California 93523-95000 (1989).